# THE FORMATION OF AMORPHOUS METALS BY LIQUID QUENCHING

Supplement to Sci. Rep. RITU, A, June, 1978

# THE FORMATION OF AMORPHOUS METALS BY LIQUID QUENCHING

Paul Hideo Shingu and Ryohei Ozaki

Department of Metal Science and Technology,

Kyoto University, Yoshida Sakyoku, Kyoto

## ABSTRACT

The experimentally estimated cooling rates of liquid metals by the liquid quenching methods are described and the attainable cooling rates are discussed. The crystal nucleation and growth during cooling of liquid metals are examined both for the case of homogeneous and heterogeneous nucleation in order to make an assessment of the critical cooling rate for the amorphous metal formation. The kinetics of crystallisation of amorphous metals studied by the dilatometry are shown and the relaxation time for the crystal nucleation is given to discuss in connection with the critical cooling rate near glass temperature.

## INTRODUCTION

In order to make the assessment if one can obtain an amorphous phase of certain alloy by liquid quenching, one should know what extent of rapidity one can attain by the technique which one employs for cooling and one should also know if the expected cooling rate is sufficient to avoid crystallisation during the course of cooling. In addition to these, one has to know the stability of the obtained amorphous phase if one expects some application of the material which can best be assessed by the knwoledge of the crystallisation kinetics.

It is the purpose of this paper to describe these three aspects of the condition concerning the formation of amorphous metals by the liquid quenching technique, namely, 1) the attainable cooling rate, 2) the critical cooling rate based on the nucleation and growth theory and 3) the kinetics of crystallisation near the glass temperature.

## [1] THE COOLING RATE OF LIQUID QUENCHED METALS

### (i) The degree of extension of solid solubility as a measure for the cooling rate.

The technique of liquid quenching in its early days of developement was used frequently to demonstrate the possibility of extension of solid solubility of binary alloys. The extent of the extension of solid solubility, hence, may be used to assess the effectiveness of various cooling methods. Fig.1 shows the measured lattice parameters plotted against the concentration of solute in Al alloys splat quenched by the gun method. Although the linear change in lattice parameter with solute concentration do not necessarily mean the extension of perfect solid solution range(1), if one assume that the solid solution is formed when Vegard's law is nearly obeyed, the result indicate that in the case of Al-Si and Al-Cu alloys the solubility is extended to nearly eutectic composition. It is evident that Al-Cu is a convenient system to use because of the large lattice parameter change due to the solid solution formation.

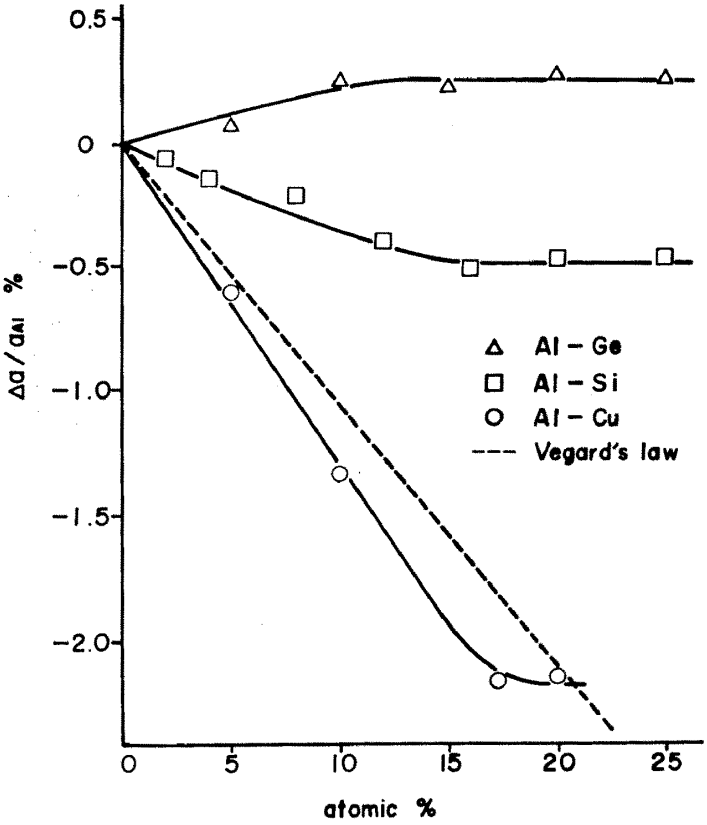


Fig.1 The lattice parameter change vs solute concentration in aluminium for specimens splat quenched by gun method.

Fig.2 shows the comparison of the effectiveness of substrate material and the splat atmosphere for the gun method. It is to be noted that quartz, which has about two orders of magnitude smaller thermal conductivity as compared with silver or copper apparently is just effective as a substrate material as far as the ability to extend the solid solubility is used as the measure. However, the better cooling capability of high thermal conductivity materials is evident since when the near eutectic Fe-C binary alloys are splat quenched, partially amorphous film can be obtained on Cu or Ag substrates but not on quartz.

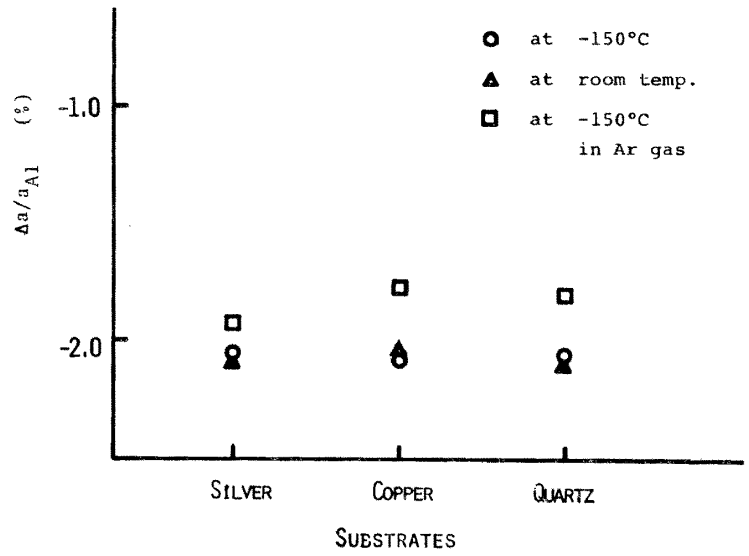


Fig.2 The lattice parameter change of Al-$CuAl_2$ eutectic alloy splat quenched by the gun method on various substrates.

In the case of splat quenching in argon gas at the substrate temperature of -150°C, the lattice parameter changes shown in Fig.2 indicate less effective cooling for all three substrates. The reason for this result is thought to be due to the vapor deposition on the substrates.

The temperature of the substrate do not affect much on the cooling effectiveness as it is seen by the comparison between the room temperature and -150°C cases in vacuum. The effect of the substrate temperature is further checked using the solubility of Si in Al as shown in Fig.3.

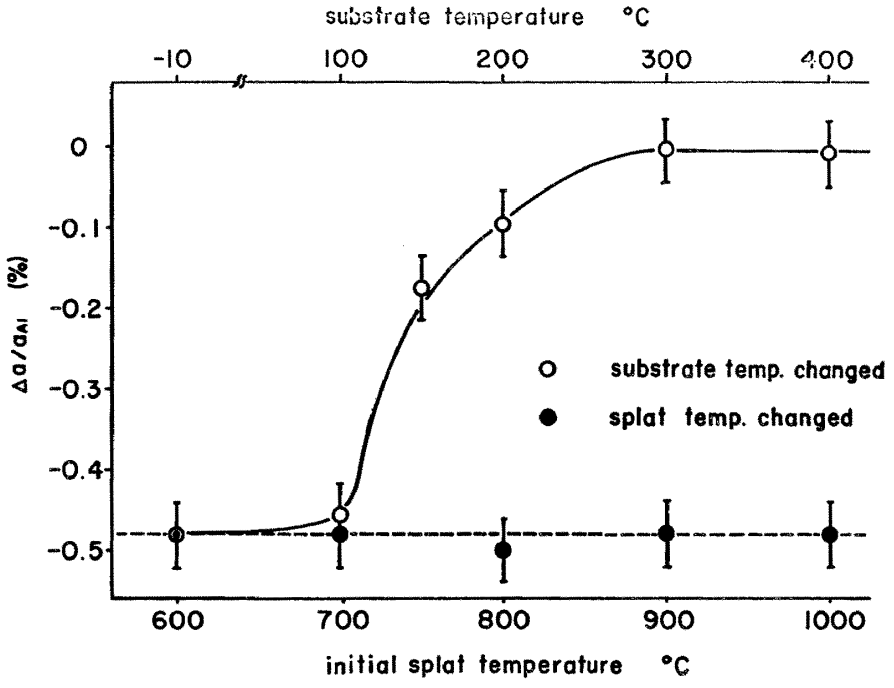


Fig.3 The effect of substrate temperature and the initial splat temperature on the solid solubility of Si in Al for the Al-12at%Si alloy splat quenched by the gun method.

The sbustrate temperature up to about 100°C shows little effect on the attainable solid solubility in this case. It is also to be noted that the maximum superheat temperature do not influence much on the attainable solid solubility.

Some trials of the lattice parameter measurements were made for specimens of Al-$CuAl_2$ eutectic alloy liquid quenched by a stainless steel single roller at a tangential velocity of about 4000cm/sec. The maximum extension of solid solubility was only 6at%Cu which is a far smaller value as compared to 17at%Cu in the case of gun method. The major reasons for the slower cooling rate for the roller method are the thicker specimen size and shorter contact time with the sbustrate.

(ii) Cooling rate evaluation by the eutectic lamella width measurement.

The width of eutectic lamella, $\lambda$, and the solidification rate, R, is related by a relation given as (2,3),

$$\lambda = AR^{-n} \qquad (1)$$

the exponent n takes the value of about 0.5. The value of A for the case of Al-$CuAl_2$ eutectic alloy is nearly $1.0\times10^{-5}$ $cm^{3/2}sec^{-1/2}$. Eq.1 is known to hold, experimentally, down to the $\lambda$ value of about $10^{-5}$cm for Al-$CuAl_2$ lamella. Examples of the photomicrographs of lamella structure and the plot of $\lambda$ vs R is given in Fig.4.

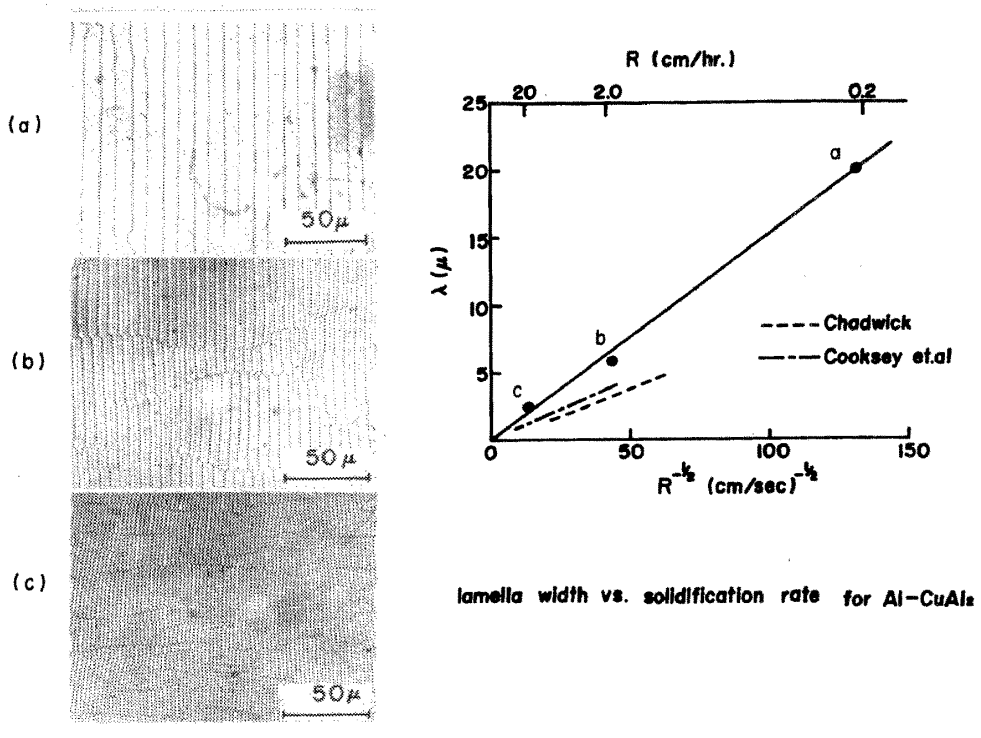


Fig.4 The width of eutectic lamella of Al-$CuAl_2$ alloy plotted against the square root of the solidification rate. The photomicrographs (a),(b) and (c) show the lamella structures obtained by the solidification conditions indicated by the same letters in the plot. The solidification direction is perpendicular to the plane of the photographs.

When the lamella width is measured for the liquid quenched lamellar eutectic specimen the solidification rate may be known by extrapolating Eq.1 and using the measured value of specimen thickness and assuming the Newtonian cooling, the heat transfer coefficient, h, between the specimen and the substrate is evaluated. Then the equation for the Newtonian cooling gives the temperature-time relation as,

$$T = T_s + ( T_o - T_s )\exp(- ht/\rho cd) \qquad (2)$$

where $T_s$: substrate temperature, $T_o$: initial splat temperature, $\rho$ : dencity, c : specific heat and d : specimen thickness.

The transmission electron micrographs of an electropolished specimen prepared from a ribbon sample of Al-$CuAl_2$ eutectic alloy liquid quenched by the single roller method is given in Photo 1.

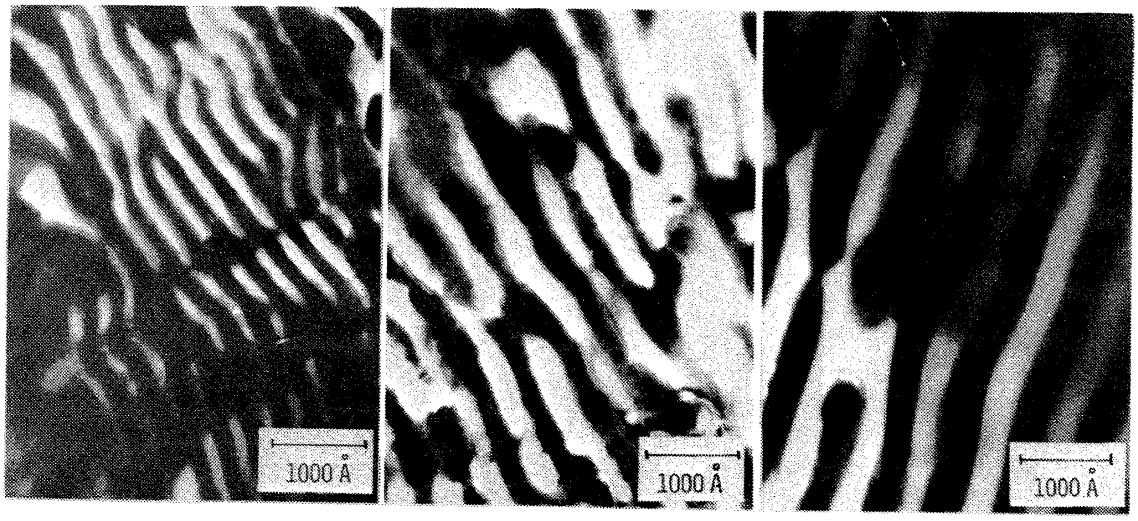


Photo 1 Transmission electron micrographs of eutectic lamellae of an Al-$CuAl_2$ sample liquid quenched by the single roller method.

The variation of lamella width for these three photographs indicates the variation in solidification rate within one sapmple. The cooling rate calculated for the smallest lamella width is in the order of $10^5$°C/sec. It is to be noted that when Fe-P-C alloys of proper composition range are liquid quenched by the same apparatus in the same condition except for the initial splat temperature, amorphous ribbons are produced.

(iii) The measurement of the cooling rate by the use of thermocouple.

Fig.5 shows a sketch of a device to measure the thermoelectricity when the liquid sample is splat quenched on a copper substrate. A thermocouple is formed by the copper substrate and a constantan wire of 0.05mm diam. The electrical contact of the couple is formed when the liquid sample is attached over the tips of these metals.

An example of the synchroscope image of the response of thermocouple during cooling of a splat quenched Al-Si alloy and the corresponding logarithmic plot of the cooling curves are shown in Figs. 6 and 7 respectively. The appearance of two cooling curves is due to the successive attachiment of separate drops of the liquid sample. The cooling rate at 300°C for curves (1) and (2) in these figures are $1.9\times10^6$ and $2.1\times10^7$ °C/sec respectively.

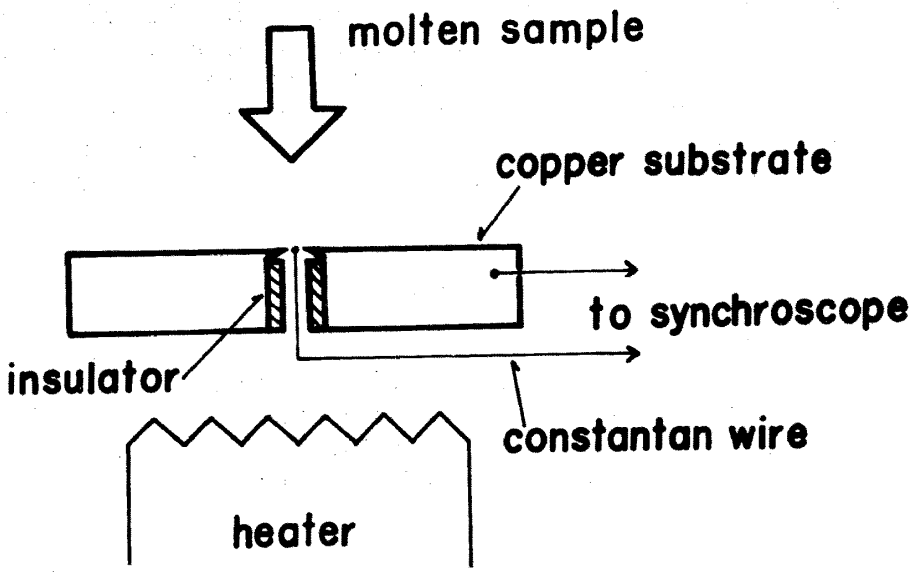


Fig.5 Schematic drawing of the device for the cooling rate mesurement.

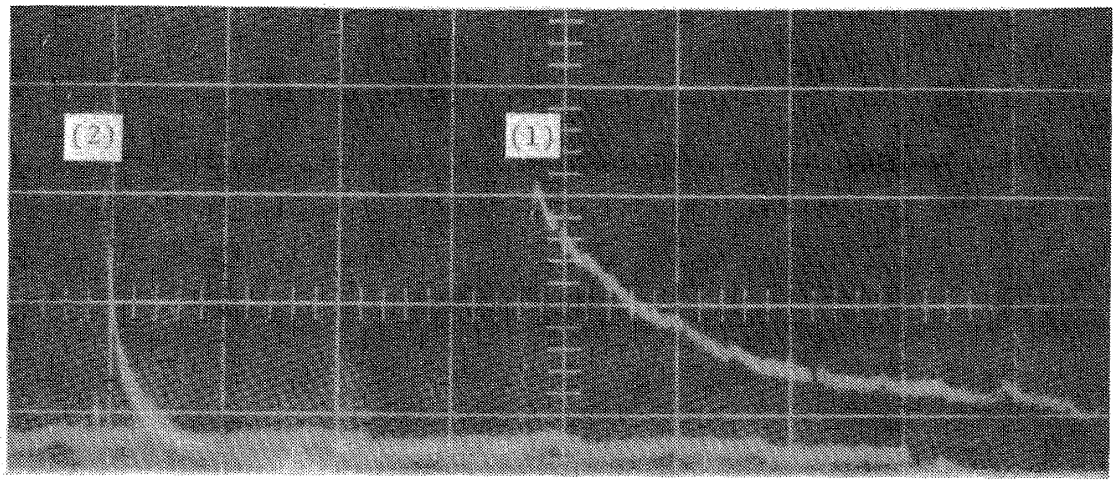


Fig.6 Synchroscope traces of thermoelectricity during cooling of splat quenched Al-Si alloy from 710°C. The smallest scales for the ordinate and abscissa are about 16°C and $10^{-5}$ sec respectively.

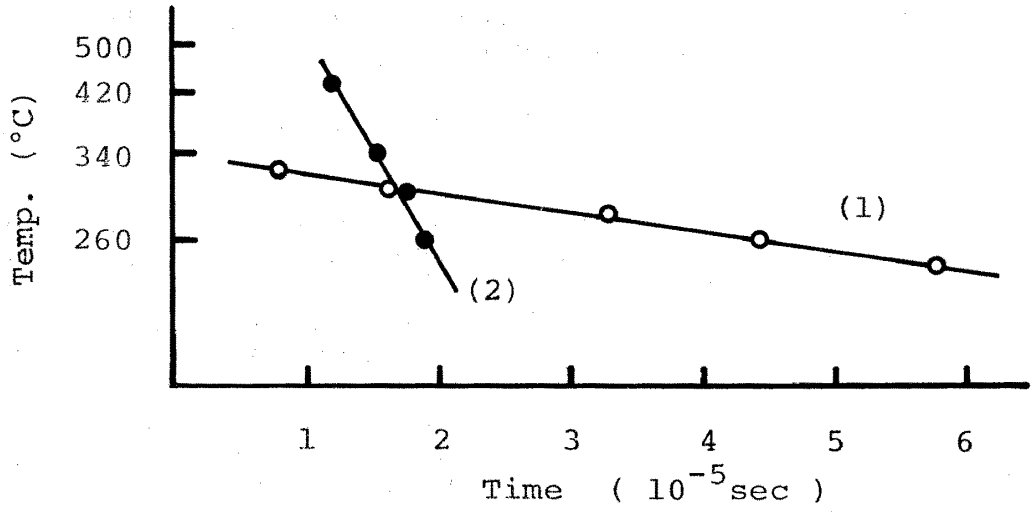


Fig.7 The plot of logT vs time for the two traces in Fig.6. Numbers (1) and (2) refer to the corresponding numbers in Fig.6.

## [2] THE CRYSTAL NUCLEATION AND GROWTH DURING LIQUID QUENCHING

The critical cooling rate to form an amorphous metal by liquid quenching may be defined as the cooling rate by which only negligible volume fraction, usually set as $10^{-5}$ or $10^{-6}$, of total sample can crystallise during cooling. Hence in order to estimate the critical cooling rate it is necessary to know the formulation of the nucleation and grwoth kinetics as a function of temperature.

The classical nucleation theory gives the following expression for the nucleation frequency(5 - 10),

$$I \simeq \frac{10^{30}}{\eta} \exp\left[ - \frac{16\pi}{3}\alpha^3\beta\left(\frac{Tr}{1-Tr}\right)^2 \right] \qquad (3)$$

where, $\eta$ : viscosity of liquid, Tr : reduced temperature = $T/T_M$, $T_M$ : equilibrium melting point, $\alpha$ : a factor which depends on the atomic arrangement at the interface with the value close to unity, $\beta$ : the entropy change due to solidification in the unit of gas constant.

The growth rate of the crystal nuclei is given by the molecular kinetic consideration assuming that the atomic transport across the interface region, which usually is assumed as several atomic diamters thick, takes place by the diffusive process as follows,

$$v = \frac{K}{\eta}( 1 - Tr ) \qquad (4)$$

where, $K = a^3L/3\pi\lambda$ , a : atomic diamter, L : heat of fusion, $\lambda$ : interface thickness.

The calculated result for the nucleation and growth rate for pure iron as a function of reduced temperature is given in Fig.8.

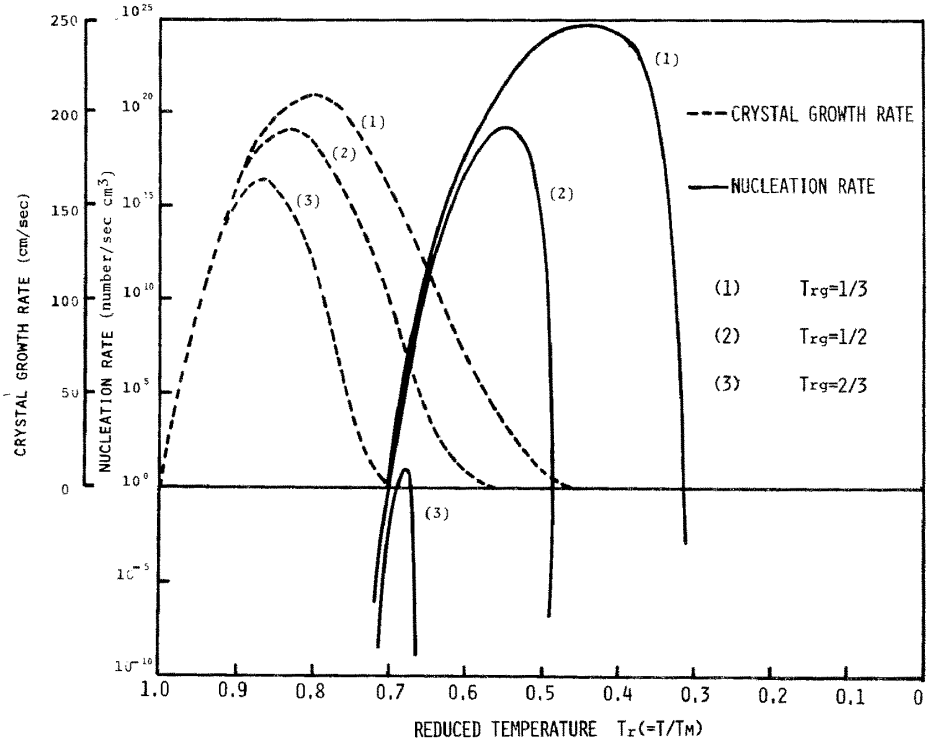


Fig.8 The calculated crystal nucleation and growth rates as a function of reduced temperature based on the Eqs. (3) and (4). $T_{rg}$s are the given glass temperatures.

Based on such temperature dependence of the nucleation and growth rate as shown in Fig.8 and assuming that these temperature dependence of kinetics to hold at any instantaneous temperature during cooling, the T-T-T (temperature-time-transformation) diagram may be drawn to visualize the critical cooling condition.

The T-T-T diagram, although it is frequenctly used to show the critical cooling rate for the amorphous metal formation, only gives the time necessary to reach a given crystallised fraction by the isothermal holding at a given temperature.

The liquid quenching is a continuous cooling process hence the critical cooling rate may better be estimated by the C-C-T (continuous-cooling-transformation) diagram which takes the cumulative effect of nucleation and growth during cooling into account.

The C-C-T diagram for a known cooling curve may be obtained from the relation,

$$-\ln(1 - x) = \frac{4\pi}{3} \int_0^t I(\theta) \left[ \int_\theta^t v(\beta) d\beta \right]^3 d\theta \qquad (5)$$

where, x : crystallised fraction, t : time after the melting point is passed during cooling.

The relation between T-T-T and C-C-T diagrams is not simple but there are methods to estimate the C-C-T diagram from the knowledge of T-T-T diagram, for example, the use of "additivity" rule which assumes the cumulative effect of incubation time consumption during cooling is additive(11) or the use of semi-empirical rule known as the Grange-Kiefer method(12).

Examples of calculated T-T-T and C-C-T diagrams for the cases of iron and $SiO_2$ are given in Figs. 9 and 10. It is to be noted that the C-C-T diagrams in these figures are for the linear continuous cooling condition.

These calculations discussed so far are based on many assumptions involved in the nucleation and growth theories. Moreover, the data for the viscosity of undercooled liquid is not known for metals hence at the present stage not too much quantitative accuracy should be expected on the calculated critical cooling rate. However, the fact that the calculated critical cooling rate for $SiO_2$, which is based on the experimental viscosity data(12,13), is in a reasonable range suggests the possibility of obtaining useful results provided the viscosity of undercooled metal liquids can be estimated with some accuracy.

Another important point about the crystallisation during cooling is the effect of heterogeneous nucleation which takes place at small undercoolings.

Fig.11 shows the temperature range of activation of heterogeneous nucleation sites during a course of slow linear cooling for the nucleation sites with various "contact angles",which is the measure of the nucleation potency of these sites.

It is well visualized that the event of nucleation completes at the temperature range near the melting point during cooling if the heterogeneous nuceation sites with small contact angles are present.

Since in the case of conventional solidification practices hardly any undercooling is experienced, considerable number of heterogeneous nucleation sites must exist in a molten metal sample. For the estimation of the critical cooling rate not only homogeneous but also heterogenous nucleation should hence be considered.

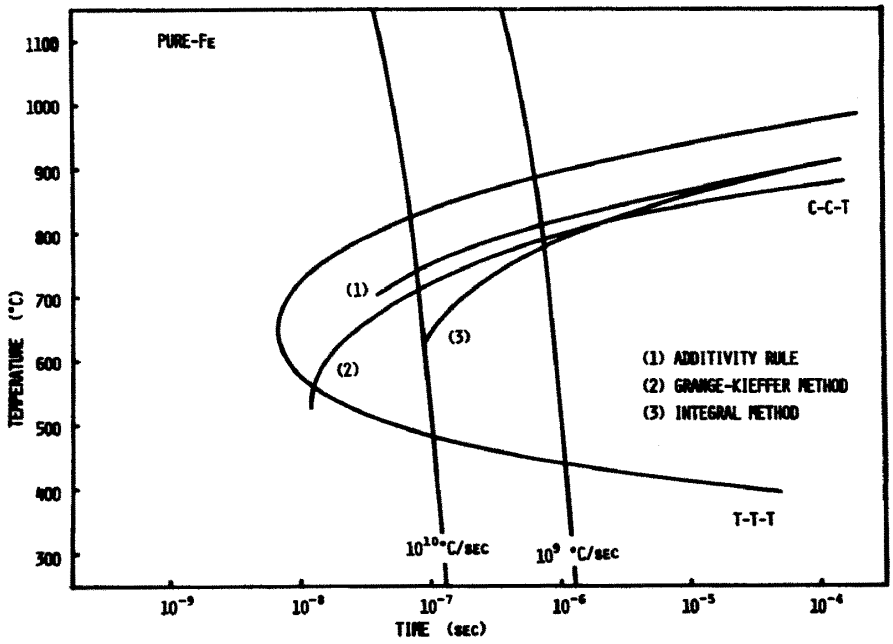


Fig.9 Calculated T-T-T and C-C-T diagrams for the crystallised fraction of $10^{-6}$ for iron. Two linear cooling curves are shown for the purpose of reference.

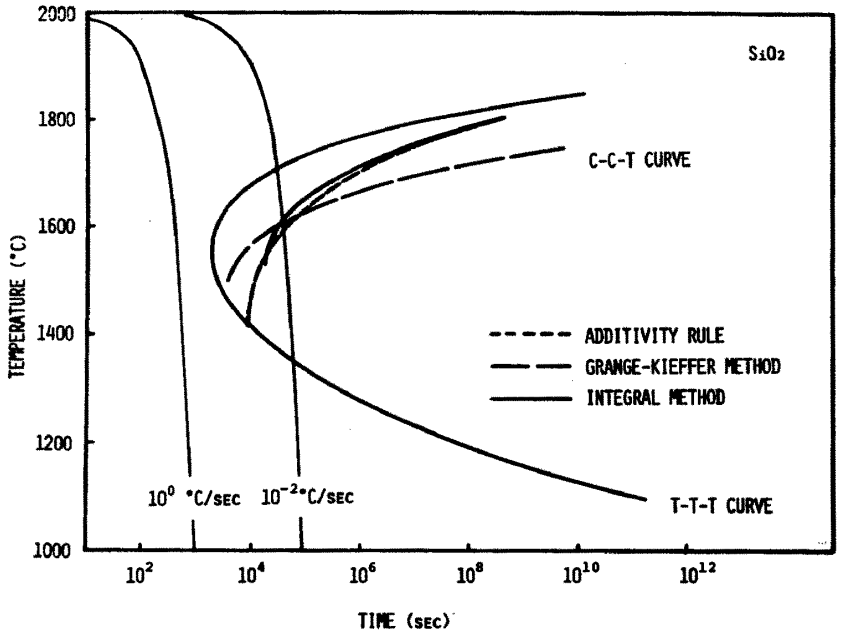


Fig.10 Calculated T-T-T and C-C-T diagrams for the crystallised fraction of $10^{-6}$ for $SiO_2$ based on the published data for the viscosity at undercooled state.

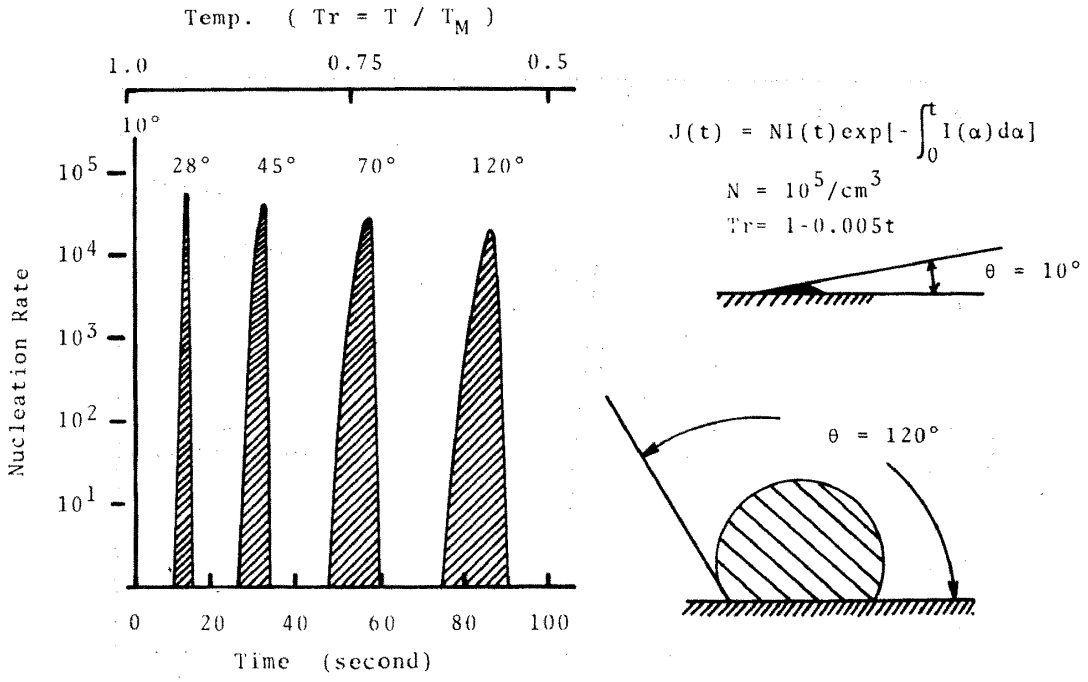


Fig.11 Calculated heterogeneous nucleation rate for iron during a linear cooling with $10^5/cm^3$ nucleation sites of different contact angle θ. Note that each hatched area in the plot equals $10^5$.

An example of the comparison of T-T-T diagrams for the homogeneous and heterogeneous nucleation is given in Fig.12.

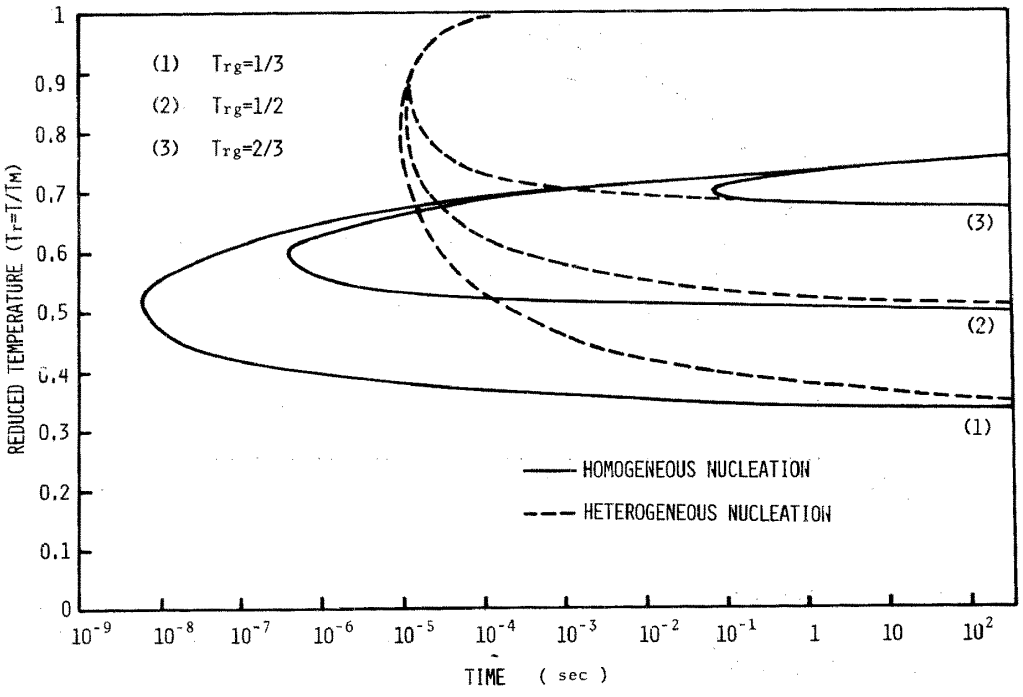


Fig.12 Comparison of T-T-T diagrams for the homogeneous and heterogeneous nucleation cases for iron. $100/cm^3$ heterogeneously nucleated crystals are given at Tr=1 for the heterogeneous nucleation case.

It is to be noted that the position of the "nose" of the T-T-T diagram for the heterogeneous nucleation case do not vary as much with the change of assumed glass temperature as it is so in the case of homogeneous nucleation. The position of the nose in T-T-T diagram for the heterogeneous nucleation case depends mainly on the maximum crystal growth rate while in the case of homogeneous nucleation, it depends mainly on the maximum nucleation rate.

Photo 2 shows an example of the micrograph of the crystal-amorphous boundary formed during liquid quenching obtained as a result of an insufficient cooling rate. The size of the crystal in the micrograph is several microns wide which is a comparable dimension with the grain size of conventionally cast samples indicating the crystal nucleation for this liquid quenched sample was heterogeneous.

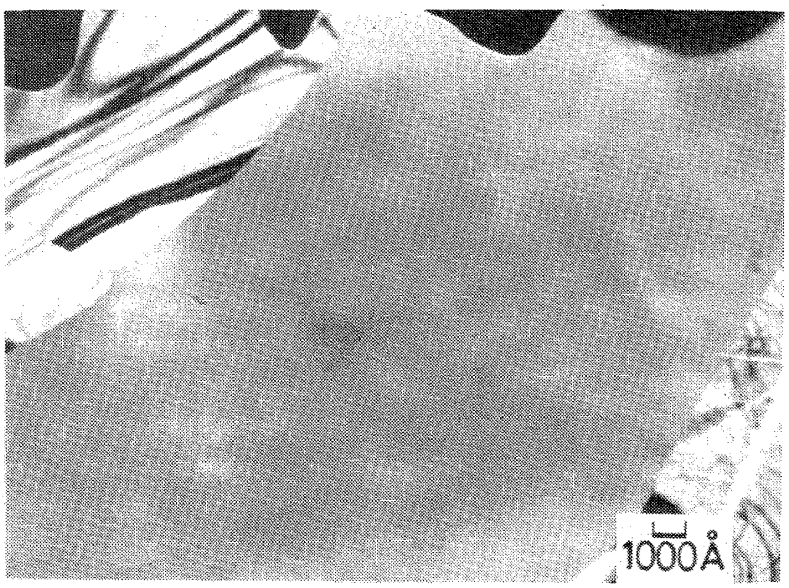


Photo 2 Transmission electron micrograph of Fe-19.7at%C alloy splat cooled by the gun method. Note the boundary of amorphous and crystalline region formed during cooling.

## [3] THE KINETICS OF CRYSTALLISATION OF AMORPHOUS METALS

The evaluation of the crystallisation rate during cooling is, as mentioned in the previous section, not easy because of the rapidity of the nucleation and growth. Hence, by studying the rate of crystallisation of successfully liquid quenched amorphous metals it is hoped to obtain some knowledge about the critical cooling condition.

The crystallisation of amorphous metals is known to take different mode depending on the heating temperatures(15). The crystalline phase which appears by heating near the glass temperature is different from that emerges during cooling. The nucleation and growth kinetics should be different for the different crystal forms. Neverthless it is still worthwhile studying the nucleation and growth of crystals in the amorphous metals near the glass temperature since it is difficult to perform a detailed investigation of undercooled liquid metals near the glass temperature.

Fig.13 shows the crystallisation behavior of an amorphous alloy, $Fe_{40}Ni_{40}P_{14}B_6$ (obtained from the Allied Chemical Co.) during isothermal holding measured by dilatometry.

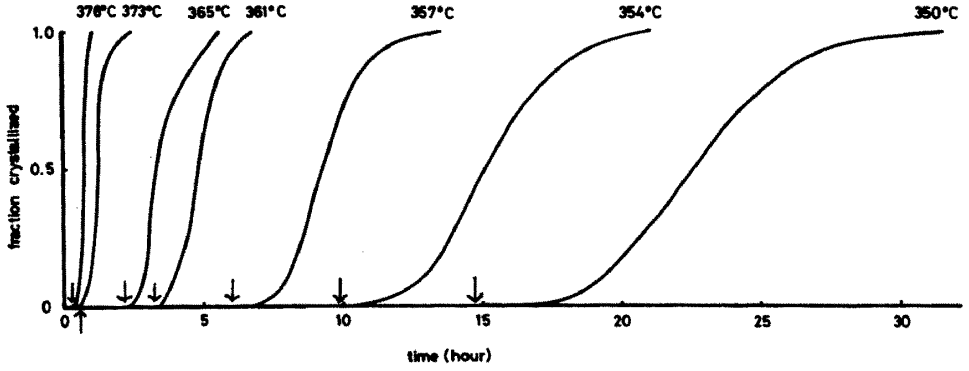


Fig.13 The fraction crystallised obtained by dilatometry plotted against the isothermal holding time for $Fe_{40}Ni_{40}P_{14}B_6$ amorphous metal. The incubation times which are interpreted as the time for nucleation obtained by fitting each curve to the straight line of slope 3 in Johnson Mehl plot are indicated by the arrows.

The crystallisation proceeds by the growth of lamella like crystals when observed by the electron microscope (16), which is characteristic of the crystallisation of high metalloid transition metal amorphous phase heated near the glass temperature. An example of which is shown in Photo 3 for the case of Fe-P-C alloy.

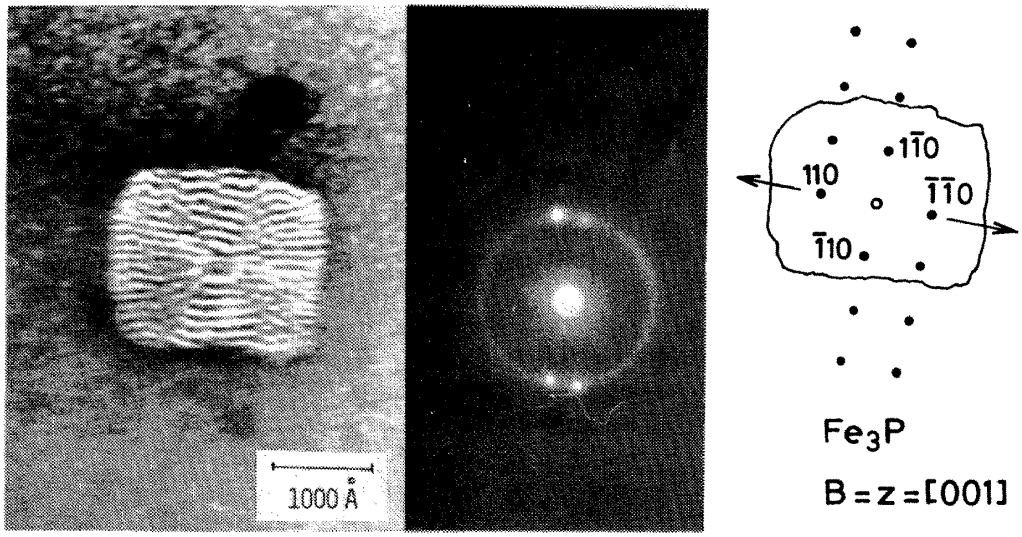


$Fe\text{-}P_{15}\text{-}C_8$ aged at 395°C for 4hr

Photo 3 Transmission electron micrograph showing the growth of a lamella crystal in the amorphous matrix. Existence of bct $Fe_3P$ phase is identified.

Since the number of crystallised region and the rate of growth of these lamella like crystals are quite steady when observed by the electron microscope at various stages of crystallisation, it is assumed that the period of nucleation and the period of growth of crystals are separable for curves shown in Fig.13.

By the theory of the kinetics of nucleation and growth, the steady state growth of eutectoid reaction may be derived from Eq.4 to give(17),

$$-\ln(1 - x) = Nvt^3 \qquad (5)$$

where N : number of crystals.

Assuming Eq.5 to hold for the period of growth, the curves of Fig.13 are fitted to the straight line with the slope of 3 in the plot of log[-log(1 - x)] vs log(t) by adjusting the time zero as shown in Fig.14.

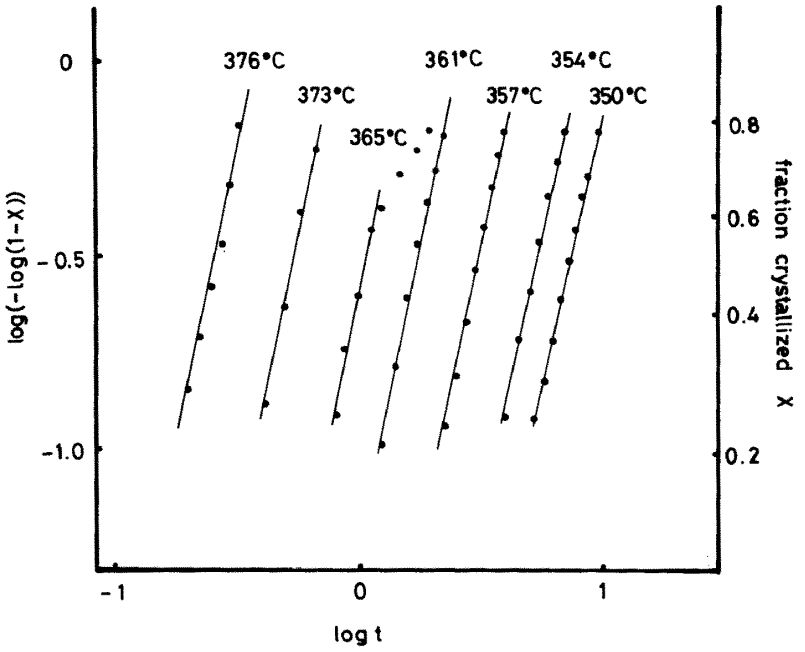


Fig.14 Johnson-Mehl plot of slope 3 to determine the time zero on the curves shown in Fig.13.

The positions of time zero obtained as a result of the adjustment to slope 3 in the plot of Fig.14 are indicated by the arrows in Fig.13.

The good fit on the straight line of slope 3 and the reasonable positions of obtained time zero, which are in all cases coincided with the time of the onset of noticeable contraction in dilatometry, verifys the validity of the assumption that the nucleation and growth processes are separable.

The plot of 1/T vs log(t) for the values of shifted positions of time zero and the time to reach x=0.5 gave good fit on straight lines giving the apparent activation energies of 105 and 103 Kcal/mol respectively.

These apparent activation energies are extraordinarily large compared with that for the phase transformation of crystalline materials. The high temperature dependence of the viscosity of the amorphous metals could be the cause for such large values of

activation energies if the nucleation and growth are limited by the rate of motion of atoms through the amorphous matrix.

The obtained temperature dependence of the nucleation time is expressed as,

$$\tau = 7.8\times10^{-33}\exp\left(\frac{105{,}000}{RT}\right) \qquad (6)$$

Eq.6 allows the extrapolation to the higher temperatures to give the information about the critical cooling condition to avoid nucleation during cooling. The calculated time for nucleation at 400,500 and 600°C are $1.02\times10^{2}$, $3.95\times10^{-3}$ and $1.56\times10^{-6}$ sec respectively which are within the attainable cooling rate as described in section 1. The extrapolation to still higher temperature is not adequate since the temperature dependence of viscosity should become small rapidly with increasing temperature.

Further studies on the variation of nucleation time with heating rate would be valuable in order to clarify the obtained large apparent activation energies for the nucleation and growth of amorphous metals.

## SUMMARY

The degree of extension of solid solubility, by the gun method of liquid quenching, up to the eutectic composition for Al-Cu alloys is possible for substrates either of Ag, Cu or fused quartz. The formation of amorphous phase of near eutectic Fe-C alloys is possible on substrates of Ag or Cu but not on fused quartz. For the case of the single roller method the maximum extension of solid solubility was 6at%Cu in Al.

The cooling rate estimated from the lamella width of Al-$CuAl_2$ for the single roller method was about $5\times10^{5}$ °C/sec. The cooling rate of an Al-Si alloy splat quenched from 710°C by the gun method measured by the thermocouple was $2.1\times10^{7}$ °C/sec at 300°C.

The estimation of the critical cooling rate for the amorphous metal formation may better be done by C-C-T diagram instead of T-T-T diagram but the information about the viscosity of undercooled liquid metals is critically needed in order to derive a quantitative result from the calculation.

Both the calculation and experimental evidence indicate the importance of heterogeneous nucleation when crystallisation takes place during cooling in liquid quenching.

Studying the kinetics of the crystallisation by the isothermal dilatometry in a temperature range of 350 to 376°C for the amorphous $Fe_{40}Ni_{40}P_{14}B_6$ alloy, the incubation time for the completion of nucleation for crystallisation was obtained as a function of temperature.

The apparent activation energy for nucleation was 105Kcal/mol. The strong temperature dependence of the viscosity of amorphous metals near the glass temperature is suggested from the obatined large value of apparent activation energy.

## REFERENCES


1) P.H.Shingu, K.Kobayashi, K.Shimomura and R.Ozaki, J.Japan Inst. Metals, 37 (1973) 433.
2) H.Burden and H.Jones, J.Inst.Metals,98 (1970) 249.
3) P.H.Shingu, A.Ohtsuki and R.Ozaki, J.Japan Inst. Metals, 37 (1973) 82.
4) R.C.Ruhl, Mater.Sci. Eng. 1 (1967).
5) D.Turnbull, J.Appl. Phys., 21 (1950) 1022.
6) G.M.Pound and V.K.LaMer, J.Am.Chem.Soc., 74 (1952) 2323.
7) Y.Miyazawa and G.M.Pound, J.Cryst.Growth,23 (1974) 45.
8) F.Spaepen, Acta Met., 23 (1975) 729.
9) P.H.Shingu and R.Ozaki,Bull.Japan Inst.Metals,15 (1976)171
10) F.Spaepen and D.Turnbull,Proc.2nd Int.Conf.on Rapidly Quenched Metals,Section 1,Ed. N.J.Grant and B.C.Giessen, MIT Press, (1976) 205.
11) J.W.Cahn, Acta Met.,4 (1956) 572.
12) R.A.Grange and J.M.Kiefer, Trans.ASM, 29 (1941) 85.
13) D.R.Uhlmann, J.Non-Cryst.Sol., 25 (1977) 43.
14) G.Hofmaier and G.Urbain, Sci.Ceram., 4 (1968) 25.
15) T.Masumoto, H.Kimura, A.Inoue and Y.Waseda, Mater.Sci.Eng. 23 (1976) 141.
16) J.L.Walter, P.Rao, E.F.Koch and S.F.Bartram, Met.Trans. 8A (1977) 1141.
17) J.W.Christian, "The theory of Transformation in Metals and Alloys" Part I,2nd.ed. Oxford Press (1975) 542.